Delineating the Eddy–Zonal Flow Interaction in the Atmospheric Circulation Response to Climate Forcing: Uniform SST Warming in an Idealized Aquaplanet Model

GANG CHEN

Department of Earth and Atmospheric Sciences, Cornell University, Ithaca, New York

JIAN LU

Center for Ocean–Land–Atmosphere Studies, and Department of Atmospheric, Oceanic and Earth Sciences, George Mason University, Fairfax, Virginia

LANTAO SUN

Department of Earth and Atmospheric Sciences, Cornell University, Ithaca, New York

(Manuscript received 10 September 2012, in final form 22 January 2013)

ABSTRACT

The mechanisms of the atmospheric response to climate forcing are analyzed using an example of uniform SST warming in an idealized aquaplanet model. A 200-member ensemble of experiments is conducted with an instantaneous uniform SST warming. The zonal mean circulation changes display a rapid poleward shift in the midlatitude eddy-driven westerlies and the edge of the Hadley cell circulation and a slow equatorward contraction of the circulation in the deep tropics. The shift of the poleward edge of the Hadley cell is predominantly controlled by the eddy momentum flux. It also shifts the eddy-driven westerlies against the surface friction, at a rate much faster than the expectation from the natural variability of the eddy-driven jet (i.e., the *e*-folding time scale of the annular mode), with much less feedback between the eddies and zonal flow.

The transient eddy–zonal flow interactions are delineated using a newly developed finite-amplitude wave activity diagnostic of Nakamura. Applying it to the transient ensemble response to uniform SST warming reveals that the eddy-driven westerlies are shifted poleward by permitting more upward wave propagation in the middle and upper troposphere rather than reducing the lower-tropospheric baroclinicity. The increased upward wave propagation is attributed to a reduction in eddy dissipation of wave activity as a result of a weaker meridional potential vorticity (PV) gradient. The reduction allows more waves to propagate away from the latitudes of baroclinic generation, which, in turn, leads to more poleward momentum flux and a poleward shift of eddy-driven winds and Hadley cell edge.

1. Introduction

Phase 3 of the Coupled Model Intercomparison Project (CMIP3) models predict robust atmospheric circulation changes under climate warming, which consequently impact the large-scale hydrological cycle. While the global hydrologic cycle is expected to intensify with increased atmospheric moisture content in a warmer climate, it is predicted that the amount of precipitation in the subtropical areas will be reduced (e.g., Held and Soden 2006). The drying at the poleward edge of the subtropical dry zones has been linked to a poleward expansion of the Hadley cell circulations (e.g., Lu et al. 2007; Seager et al. 2007), and is associated with a trend toward the positive phase of annular modes (e.g., Previdi and Liepert 2007). In the extratropics, precipitation along the midlatitude storm tracks is projected to shift poleward in both hemispheres (e.g., Yin 2005; Lorenz and DeWeaver 2007a). Understanding the cause for the circulation shift is critical for the prediction of subtropical and midlatitude climate change.

A number of hypotheses have been put forward to explain the circulation changes predicted in the CMIP3 models. The root cause has generally been traced back to the enhanced upper-tropospheric warming with greenhouse

Corresponding author address: Gang Chen, Bradfield 1115, Dept. of Earth and Atmospheric Sciences, Cornell University, Ithaca, NY 14853.
E-mail: gc352@cornell.edu

DOI: 10.1175/JAS-D-12-0248.1

gas warming, as expected from the moist adiabatic adjustment to surface warming. However, individual studies focus on different, albeit often related, aspects of atmospheric dynamics. The poleward expansion of the Hadley cells has been attributed to the increased subtropical tropopause height and increased subtropical static stability (Lu et al. 2007; Frierson et al. 2007) and baroclinic adjustment toward constant subtropical supercriticality (Korty and Schneider 2008). The poleward shift of the storm tracks has been explained by a rise in the extratropical tropopause height (Lorenz and DeWeaver 2007b), a change in the meridional wave propagation associated with increases in eddy phase speed (Chen and Held 2007; Chen et al. 2008), eddy length scale (Kidston et al. 2011) or barotropic instability (Kidston and Vallis 2012), a change in the baroclinic instability due to enhanced midlatitude static stability (Lu et al. 2008, 2010) or isentropic slope (Butler et al. 2011), a change in the baroclinic eddy life cycle owing to stronger lower-stratospheric wind shear (Wittman et al. 2007) or increased eddy length scale (Rivière 2011), and a change in the poleward energy transport (e.g., Frierson et al. 2006; Cai and Tung 2012). Although most studies have used both simple and comprehensive models to support their hypotheses, there is not a general approach to delineate the eddy–zonal flow interaction in response to external climate forcing, and therefore it is difficult to detect the most essential mechanism(s) for the circulation changes under global warming.

Of particular concern to the current study is how a uniform SST warming, with similar impacts as global warming, can influence the atmospheric circulation in a fundamental way. To dissect the key processes in the atmospheric response to SST warming, we utilize a super-ensemble method [also used in Wu et al. (2011) for doubling CO_2]—running a large number of ensemble experiments with a ''switch on'' climate forcing and analyzing the transient eddy–zonal flow responses. Without the loss of generality, we choose to focus on the atmospheric response to prescribed zonally symmetric sea surface temperature (SST) forcing in an aquaplanet atmospheric model. Thus, we ignore the changes of stationary waves (Joseph et al. 2004), but retain all the dry and moist dynamics that have been considered in the previous studies. Given that the atmospheric circulations have shifted poleward in both hemispheres under climate warming while the changes of surface temperature gradient are opposite in the two hemispheres, we choose a uniform SST warming as the forcing. The sensitivities of the storm tracks and zonal circulations to the mean SST or the SST gradient have been previously documented (e.g., Caballero 2005; Frierson et al. 2007; Brayshaw et al. 2008; Medeiros et al. 2008; Kodama and Iwasaki 2009; Lu et al. 2010; Chen et al. 2010).

The extratropical circulation changes under climate warming have been explicated in terms of annular modes—the leading modes of extratropical variability (e.g., Miller et al. 2006). The fluctuation–dissipation theorem (Leith 1975) predicts that the climate response is proportional to the projection of the climate forcing onto the dominant mode of climate variability multiplied by the decorrelation time scale of the mode. Studies with idealized atmospheric models showed that the annular mode is the preferred climate response to arbitrary mechanical and thermal forcings, and that the response is indeed proportional to the projection of external forcings [e.g., the effective torque to the zonal wind defined by Ring and Plumb (2008)] onto the annular mode (Ring and Plumb 2007, 2008; Gerber et al. 2008; Chen and Plumb 2009). In the CMIP3 models, the intermodel spread of the shift of Southern Hemisphere surface westerlies under climate warming is correlated with the *e*-folding time scale of the southern annular mode (SAM) (Kidston and Gerber 2010; Barnes and Hartmann 2010). A similar relationship was also observed in a climate model under different ocean–atmosphere coupling or partial coupling configurations (Lu and Zhao 2012). Nevertheless, a quantitative disagreement exists between the predicted and simulated annular mode changes, even for a simple system of the vertically averaged zonal winds (Chen and Plumb 2009). Further, while the fluctuation–dissipation theorem has been demonstrated useful in short-term weather predictions (e.g., Newman and Sardeshmukh 2008), it remains to be shown whether the transient adjustment of the annular mode to an instantaneous climate forcing will follow the *e*-folding time scale of the unforced annular mode variability.

Generally speaking, the latitudinal shift of midlatitude westerlies can be accounted for by the change of the convergence of eddy momentum flux against the surface friction (e.g., Chen et al. 2007). A quantitative framework for the relationship between the annular mode–like response and the external forcing is usually established through projections of the momentum equation onto the annular mode (e.g., Lorenz and Hartmann 2001; Ring and Plumb 2008; Gerber et al. 2008; Chen and Plumb 2009). Additionally, the change of eddy momentum flux can be quantified from the pseudomomentum [or wave activity; see Edmon et al. (1980) or Andrews et al. (1987) for details] budget of the atmosphere. The pseudomomentum budget of a barotropic model has been used to explain the structure and persistence of annular modes (Vallis et al. 2004; Barnes et al. 2010), but problems remain in defining pseudomomentum for finite-amplitude waves in the regions of zero absolute vorticity gradient, as well as in reconciling a stirred barotropic system with a baroclinic system. Recently, Nakamura and Zhu (2010)

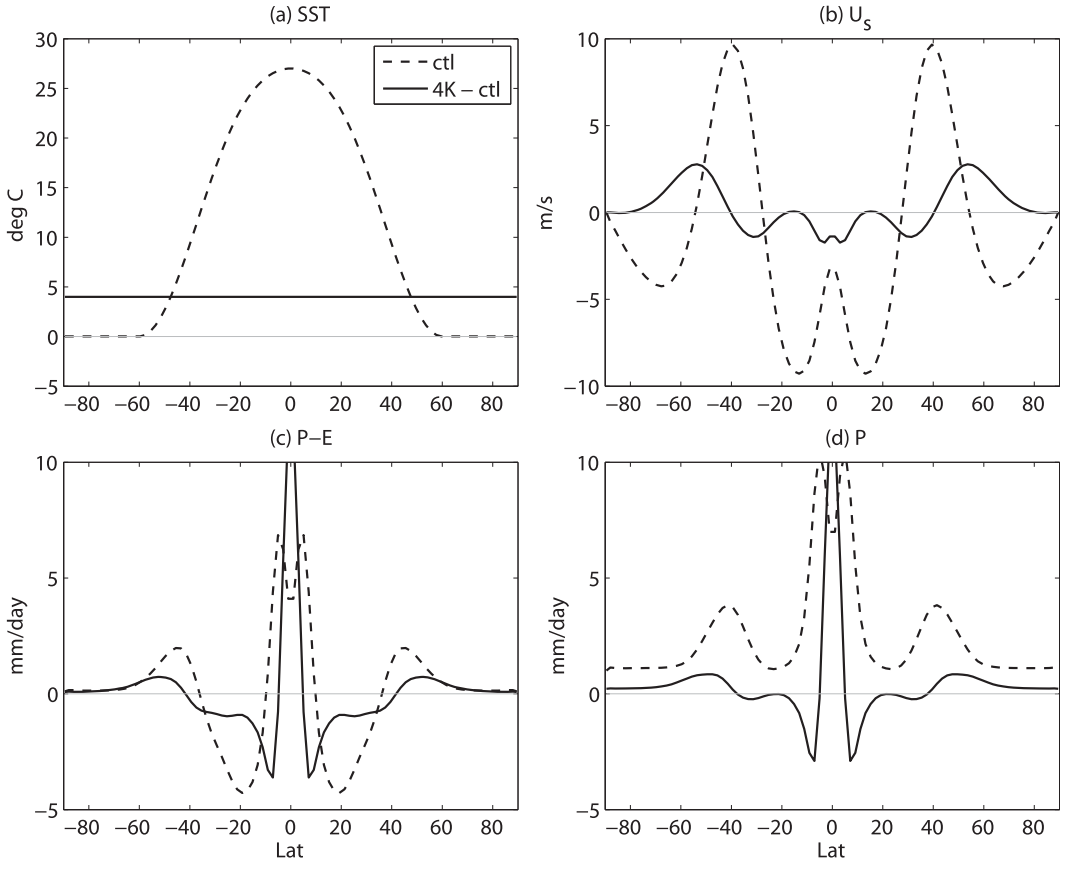

FIG. 1. Zonally averaged climatologies (dashed) and equilibrated responses to 4-K uniform SST warming (solid) as a function of latitude: (a) prescribed SST, (b) surface ($\sigma = 0.996$) zonal wind, (c) precipitation minus evaporation ($P - E$), and (d) precipitation.

and Nakamura and Solomon (2010) developed a quasi-geostrophic (QG) pseudomomentum formalism for finite-amplitude wave activity based on basic conservation principles. This formalism, by considering the conservation of modified Lagrangian mean (MLM) potential vorticity (PV), holds for both small- and finite-amplitude eddies. It now becomes viable to construct a physically rigorous framework to diagnose the causes for the changes of baroclinic waves during the annular mode–like adjustment to an imposed SST forcing.

In this paper, the transient atmospheric circulation changes with a uniform SST warming are analyzed from the perspectives of the annular mode and pseudomomentum budget. In section 2, we describe the aquaplanet model and experiment setup. In section 3, the equilibrated and transient atmospheric circulation responses to a uniform SST warming are depicted. The cause of the circulation change is then diagnosed by combining the modal projection and the pseudomomentum budget in section 4. We offer a discussion on various mechanisms of the circulation shift in section 5 and conclude with a summary in section 6.

2. The aquaplanet model and experiment setup

We use the aquaplanet version of the Geophysical Fluid Dynamics Laboratory (GFDL) Atmospheric Model, version 2.1 (AM2.1) (Delworth et al. 2006), following the idealized configurations described in the aquaplanet model benchmark (Neale and Hoskins 2000). The control SST (Qobs SST) profile is specified as a function of latitude $T_s(\phi) = 27\{1 - 0.5\sin^2(3\phi/2) - 0.5\sin^4(3\phi/2)\}$°C for $-\pi/3 < \phi < \pi/3$ and 0°C otherwise (i.e., the dashed line in Fig. 1a), and there is no sea ice in the model. The solar radiative forcing is fixed in the equinoctial condition. As the prescribed SST and radiative forcings are zonally symmetric, there are no stationary waves in the model, yet there are transient eddies arising from baroclinic instability. Since the forcings are symmetric about the equator, the time-mean or ensemble-mean results are averaged over the two hemispheres.

Previous studies (e.g., Caballero 2005; Frierson et al. 2007; Brayshaw et al. 2008; Medeiros et al. 2008; Kodama and Iwasaki 2009; Lu et al. 2010; Chen et al. 2010) have explored the circulation regimes for different SST structures. For example, the Hadley cell expands and the eddy-driven jet moves poleward with enhanced global mean temperature (Frierson et al. 2007; Lu et al. 2010). When the SST gradient is altered, the jet moves toward (away from) the flank where baroclinic wave generation is enhanced (reduced) because of an increase (decrease) of anomalous SST gradient (Chen et al. 2010). Here we focus on a simple forcing—raising the SST everywhere by 4 K from the control SST profile with both equilibrated and transient simulations. A sensitivity study with respect to the magnitude of warming has confirmed that the extratropical circulation responses are approximately linear to the strength of forcing for the control climate examined, although the tropical precipitation change can be as large as the mean precipitation in magnitude, leading to a change in the ITCZ structure (cf. Figs. 1d and 3 and section 3a). In the equilibrated runs, the results are analyzed from the last 8000 days of control and perturbed integrations. In the transient runs, a 200-member ensemble of realizations is formed by branching out from the last day of each month of the control simulation. The SST in each realization is perturbed instantaneously, and the model is integrated forward for 180 days.

3. Equilibrated and transient atmospheric responses to uniform SST warming

a. Equilibrated atmospheric responses

Despite the simplicity of uniform SST warming, the aquaplanet model captures many robust features of the circulation and hydrological cycle changes under global warming in CMIP3 models. Figure 1 shows the equilibrated changes in the zonally averaged surface (lowest model level $\sigma = p/p_s = 0.996$) zonal wind, precipitation minus evaporation ($P - E$), and precipitation (P). While the uniform SST warming introduces no change in the surface temperature gradient, the midlatitude westerly winds and associated eddy-driven jets are displaced poleward, and the tropical and midlatitude wet regions (around the $P - E$ or P maxima) become wetter and the subtropical dry regions (around the $P - E$ or P minima) get drier. These features agree well with the circulation changes (e.g., Yin 2005) and hydrological cycle (e.g., Held and Soden 2006) changes under global warming in CMIP3 models.

The subtropical and midlatitude precipitation changes can be separately explained by the thermodynamical and dynamical mechanisms. On the one hand, Held and Soden (2006) argued that assuming no changes in atmospheric circulation, the mean hydrological cycle is simply enhanced with increased atmospheric water vapor, which in turn is controlled by the surface temperature through the Clausius–Clayperon relationship, that is, $\delta(P - E) \approx 0.07\delta T(P - E)$. Given uniform δT, the shape differences of $\delta(P - E)$ and $P - E$ implicate important dynamical changes. On the other hand, a poleward expansion of the Hadley cell circulation (Lu et al. 2007) and a poleward shift of midlatitude storm tracks (Yin 2005) can contribute to the changes in the subtropical dry zones and midlatitude precipitation. Particularly, the equatorward and poleward edges of the subtropical dry zones, where $P - E = 0$ (the dashed line in Fig. 1c), have widened, and this suggests that the simple thermodynamic argument alone is insufficient to describe the total $P - E$ response.

The vertical structures of zonal mean circulation changes in the aquaplanet simulation (Fig. 2) also resemble the circulation changes under global warming (e.g., Lu et al. 2008). The zonal mean temperature shows substantial tropospheric warming and minor stratospheric cooling,[1] with enhanced upper-tropospheric warming. This is broadly consistent with increased upper-tropospheric baroclinicity, increased tropospheric static stability (e.g., Frierson 2006), and rising tropopause height (e.g., Lorenz and DeWeaver 2007b) in CMIP3 models. The zonal wind exhibits a coherent poleward shift in the middle and lower troposphere and a strengthening on the jet's two flanks in the upper troposphere, indicating a separation between the subtropical and eddy-driven jets. In the mean meridional circulation (MMC), the rising branch of the Hadley cells has largely intensified and narrowed, but the subtropical descending branch is expanded poleward, consistent with the widening of subtropical dry zones seen in $P - E$ or P (Fig. 1). The midlatitude Ferrel circulations move together with the shift of eddy-driven westerlies.

It is noteworthy that the ITCZ changes from a double-ITCZ structure to a single-ITCZ structure in response to 4-K warming (Fig. 1d), and therefore the precipitation change is comparable in magnitude to the mean precipitation in the control run. When the amplitude of SST warming is reduced in Fig. 3, the equatorial precipitation decreases almost linearly but does not always lead to a structural change from a double to single ITCZ. Furthermore, while the subtropical and extratropical changes are robust with different models, the change

[1] As there is no change in the CO_2 concentration, the minor stratospheric cooling has to be attributed to a dynamical cause, and it could provide additional cooling to the stratospheric radiative cooling of CO_2 under climate warming (e.g., Sigmond et al. 2004).

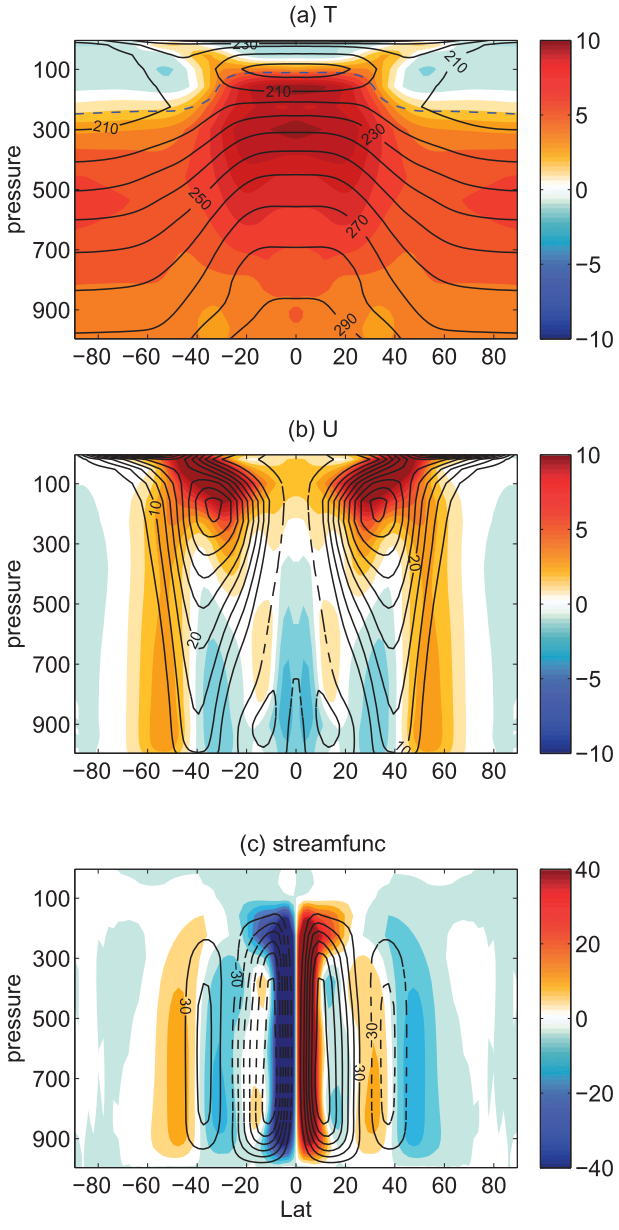

FIG. 2. Zonally averaged climatologies (contours) and equilibrated responses to 4-K uniform SST warming (shading) as a function of pressure and latitude: (a) temperature (K; dashed line indicates the tropopause), (b) zonal wind ($m\,s^{-1}$), and (c) meridional streamfunction ($10^9\,kg\,s^{-1}$).

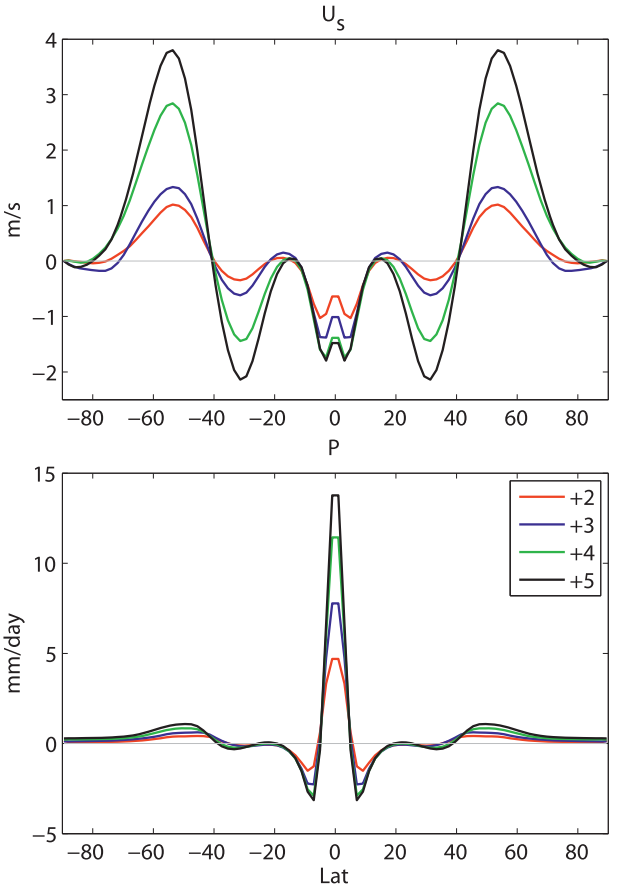

FIG. 3. Sensitivities of zonal mean (top) surface wind and (bottom) precipitation responses to the magnitude of uniform SST warming ranging from 2 to 5 K. This corresponds to the solid lines in Figs. 1b and 1d, respectively.

of the Hadley cell circulation in the deep tropics varies with models (cf. Medeiros et al. 2008), which is implicative of a strong dependence of equatorial circulation on the model's convective or cloud parameterizations as well as water vapor feedback. In more realistic models, the ITCZ can be also affected by the equatorial atmosphere–ocean coupling. Given that the ITCZ change in this type of model is likely model dependent and yet the subtropical and extratropical changes are robust (I. Held 2011, personal communication), we focus on the mechanism of the subtropical and extratropical changes.

b. *Transient atmospheric responses*

The transient atmospheric responses are investigated through an initial value approach: a large (200 member) ensemble of transient simulations with switch-on SST warming. We first show the latitudinal changes of the surface zonal wind, $P - E$, and 500-hPa MMC in time by the latitudes of the tropical extremum (see the easterly maximum in Fig. 1b for an example), the subtropical zero crossing, and the midlatitude extremum (e.g., westerly maximum). The latitudinal changes are normalized by the absolute value of the equilibrated changes to compare different variables and locations:

$$\delta\phi(t) = \frac{\phi(t) - \phi_{\mathrm{ctl}}}{|\phi_{\mathrm{equ}} - \phi_{\mathrm{ctl}}|}\,\mathrm{sign}\{\phi(t)\}\,. \qquad (1)$$

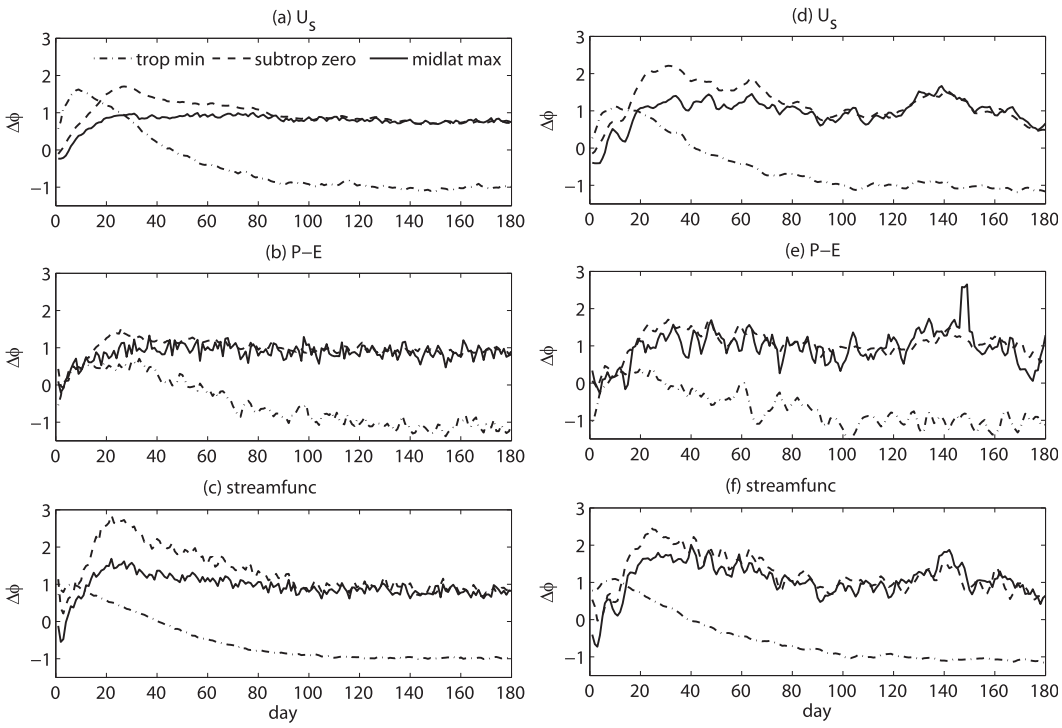

FIG. 4. The ensemble-mean transient responses to instantaneous (a)–(c) 4- and (d)–(f) 2-K uniform SST warming for changes in latitude of (top) surface wind, (middle) $P - E$, and (bottom) 500-hPa meridional streamfunction for the tropical extremum (dashed–dotted), subtropical zero crossing (dashed), and midlatitude extremum (solid). The latitudinal changes are normalized by the absolute value of the equilibrated changes [Eq. (1)] such that a positive value denotes a poleward shift and unity denotes the same magnitude of change as the equilibrated change. Note that other figures of transient evolution show the first 60 days of the entire 180 days.

Here a positive (negative) value of $\delta\phi(t)$ denotes a poleward (equatorward) shift and a unity denotes the same magnitude of movement in latitude as the equilibrated change.

We first test the linearity of the transient simulations with the amplitude of SST warming. Figure 4 shows the temporal change of the latitudinal indices of circulation for 4-K uniform warming in the left column and 2-K uniform warming in the right column. After the normalization with the equilibrium changes, the temporal evolution of these circulation indices shows very little sensitivity to the amplitude of the forcing, especially during the initial 60 days when the changes of the circulation indices are largest. The variability in the 2-K warming case is larger as expected from a greater noise-to-signal ratio. More importantly, as the ITCZ remains as a double-ITCZ structure with 2-K warming (cf. the equilibrium changes in Figs. 1d and 3), this confirms that the equilibrated change from a double-ITCZ structure to a single-ITCZ structure with 4-K warming has little to do with the extratropical circulation changes in our model. For the rest of the paper, we only discuss the results with the 4-K uniform warming.

The model simulations show that the profiles of surface wind, $P - E$, and midtropospheric MMC move in tandem as a whole (Fig. 4). The latitudes of midlatitude westerlies, $P - E$ maximum, and Ferrel cell (solid lines) vary from zero to unity almost exponentially, and stay nearly constant after about day 30. By contrast, the latitudes of tropical easterlies, $P - E$ minimum, and the upward branch of the Hadley cell (dashed–dotted lines) expand poleward rapidly for about a week, and then contract equatorward very slowly up to more than 100 days. The subtropical zero-crossing latitudes can be thought of as a combination of a rapid poleward drift of westerly winds and a gradual equatorward movement of easterly winds, the former being the result of midlatitude eddies and the latter forced by the ITCZ-related heating. The equilibrated changes of the subtropical zero crossings are dominated by the poleward midlatitude shift. This competition for influence between the tropical and extratropical sources is reflected in the somewhat different evolutions of the subtropical zero crossings from those of the midlatitude maxima.

The ensemble-mean and zonal mean circulation changes are plotted as a function of latitude for the first

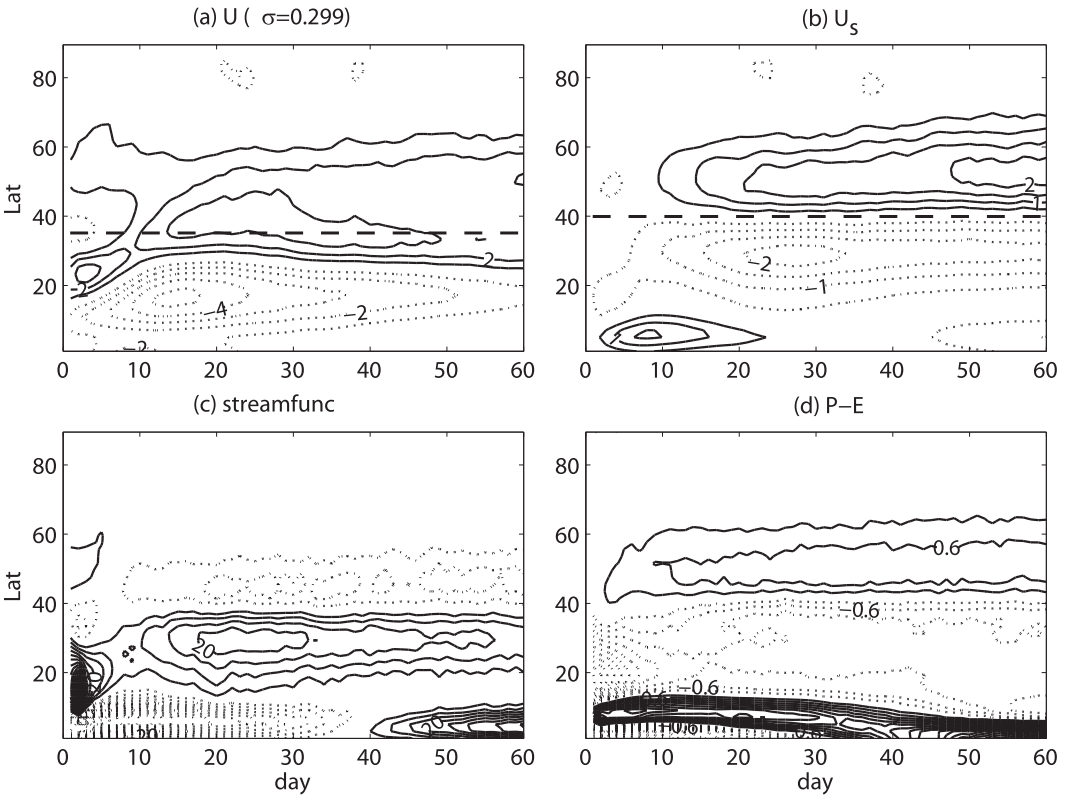

FIG. 5. Zonal and ensemble-mean transient responses to instantaneous SST warming as a function of latitude and time: (a) upper-tropospheric zonal wind ($m\,s^{-1}$), (b) surface zonal wind ($m\,s^{-1}$), (c) midtropospheric (500 hPa) meridional streamfunction ($10^9\,kg\,s^{-1}$), and (d) $P - E$ ($mm\,day^{-1}$). The dashed line in (a),(b) indicates the latitude of the westerly wind maximum in the control run.

60 days in Fig. 5, and the vertical structures of circulation changes for selected periods are highlighted in Fig. 6. The transient changes can be roughly divided into two stages by the timing of surface westerly shift (Fig. 5). In the first stage (less than about 10 days), the MMC is weakened at the equator and intensified considerably at 10°–20° latitudes, as expected from increased convective heating with surface warming (note that the mean ITCZ in Fig. 1c is located off the equator). The strengthened overturning MMC leads to increased poleward angular momentum transport in the upper troposphere and a stronger subtropical jet and more equatorward water vapor transport near the surface and drier subtropics. Interestingly, as the subtropical subsidence increases, the subtropical static stability is enhanced sharply during days 5–9, while the upper-tropospheric zonal wind is accelerated on both flanks of the mean jet (Fig. 6).

Most poleward expansions of the Hadley cell and surface zonal wind take place in the second stage after about 10 days. In the lower troposphere, the shift of surface zonal wind resembles (with opposite sign) the change of the overturning MMC, which can be explained by the balance between the surface friction and Coriolis force. The change of $P - E$ is consistent with the pattern of surface zonal mean circulation changes, but the midlatitude moist fluxes are controlled by not only the mean circulation but also the eddy fluxes. In the upper troposphere, the zonal wind is accelerated on the poleward flank of the jet stream with an extension to the surface. Additionally, the jet is accelerated on the equatorward flank, opposite to the middle- and lower-tropospheric deceleration below, leading to a separation between the subtropical jet and eddy-driven jet. Also note that the poleward shift of the eddy-driven surface westerly wind occurs before day 30, while the equatorward retreat of the subtropical jet continues after day 60 (Fig. 5). Particularly, the anomalous MMC changes within 10° latitudes switch from negative during days 25–30 to positive during days 50–60, while the extratropical circulation exhibits little changes (Fig. 6). As such, the transient response to a uniform surface warming in the second stage can be described as a fast poleward shift in the midlatitude eddy-driven jet and a slow equatorward contraction of the subtropical thermally driven jet.

The different response time scales of the eddy-driven and subtropical jets can be useful in separating the

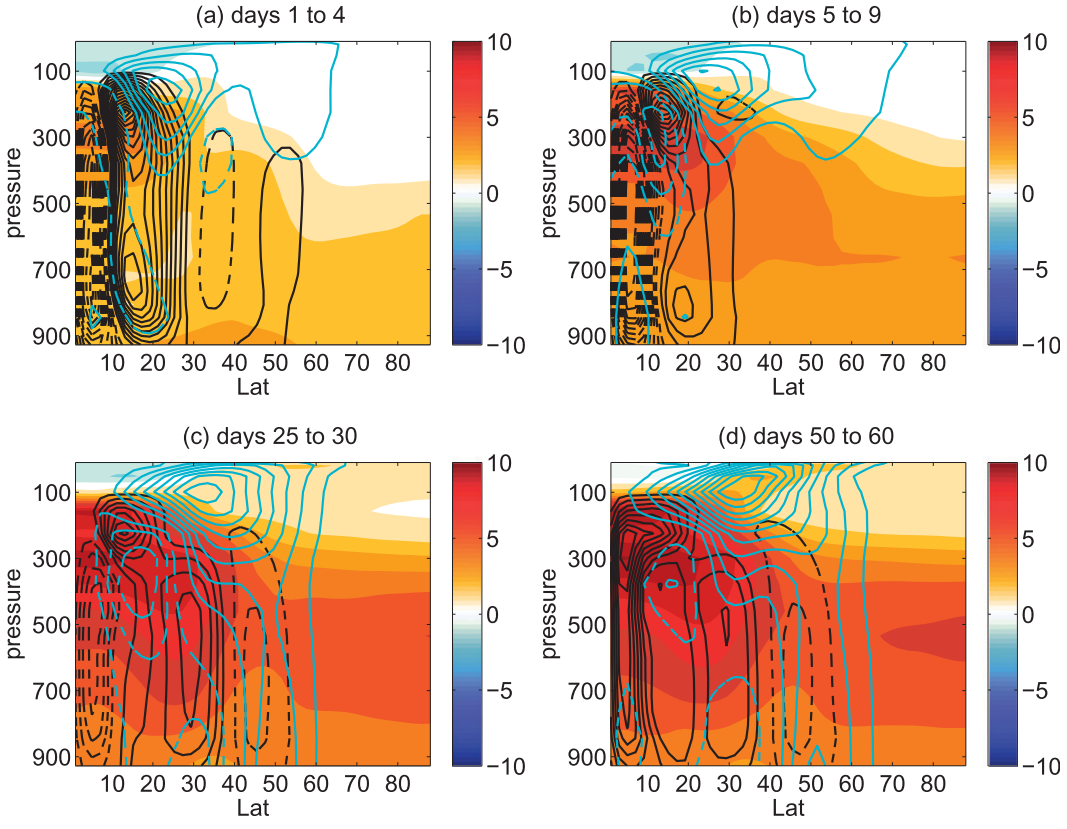

FIG. 6. Zonal and ensemble-mean transient responses to instantaneous SST warming as a function of latitude and pressure averaged for days (a) 1–4, (b) 5–9, (c) 25–30, and (d) 50–60: anomalous temperature (K; shading), zonal wind (contour interval of 1 m s^{-1}; cyan), and meridional streamfunction (contour interval of 5×10^9 kg s^{-1}; black).

hydrological cycle changes at different latitudes. Most of subtropical and midlatitude (poleward of about 20°) MMC and $P - E$ changes (i.e., subtropical drying and midlatitude shift) are associated with the midlatitude shifts. The tropical (equatorward of about 20°) MMC and $P - E$ changes (i.e., the equatorward shift in the ITCZ) are accompanied by the equatorward subtropical jet contraction.

4. Delineating the causality of the eddy–zonal flow interaction in the transient responses

a. *The changes of MMC*

The zonal mean momentum budget of the atmosphere can be written as

$$\frac{\partial \overline{u}}{\partial t} = (f + \overline{\zeta})\overline{v} - \overline{\omega}\frac{\partial \overline{u}}{\partial p} - \frac{1}{a\cos^2\phi}\frac{\partial(\overline{v'u'}\cos^2\phi)}{\partial \phi} - \frac{\partial(\overline{\omega'u'})}{\partial p} - \overline{F}, \tag{2}$$

where overbars denote the zonal means, primes denote the deviations from zonal mean, F denotes the surface friction, and other symbols follow meteorological conventions. Making the small Rossby number approximation ($f \gg \overline{\zeta}$) and small aspect ratio approximation (i.e., the ω terms are smaller than the corresponding horizontal terms), the MMC at the midtropospheric level can be diagnosed as

$$\Psi_{500} \equiv \frac{2\pi a\cos\phi}{g} p_{500}\langle \overline{v}\rangle_U \approx \frac{2\pi a\cos\phi}{g}\frac{p_{500}}{f}\left\{\frac{\partial\langle \overline{u}\rangle_U}{\partial t} + \frac{1}{a\cos^2\phi}\frac{\partial(\langle \overline{v'u'}\rangle_U \cos^2\phi)}{\partial\phi}\right\}, \tag{3}$$

where the subscript U denotes an average from the top of the atmosphere to $p_{500} = 500$ hPa and the upper-tropospheric average of X is denoted as $\langle X\rangle_U = (1/p_{500})\int_0^{p_{500}} X\, dp$.

Figure 7 shows the 500-hPa MMC (Fig. 7a) simulated in the model in comparison with the MMC (Fig. 7b) diagnosed from the momentum budget above. While the two disagree in the tropics equatorward of 20° owing to a large Rossby number and nonlinear Hadley circulation dynamics (e.g., Held and Hou 1980), the momentum budget provides a strong constraint on the MMC poleward

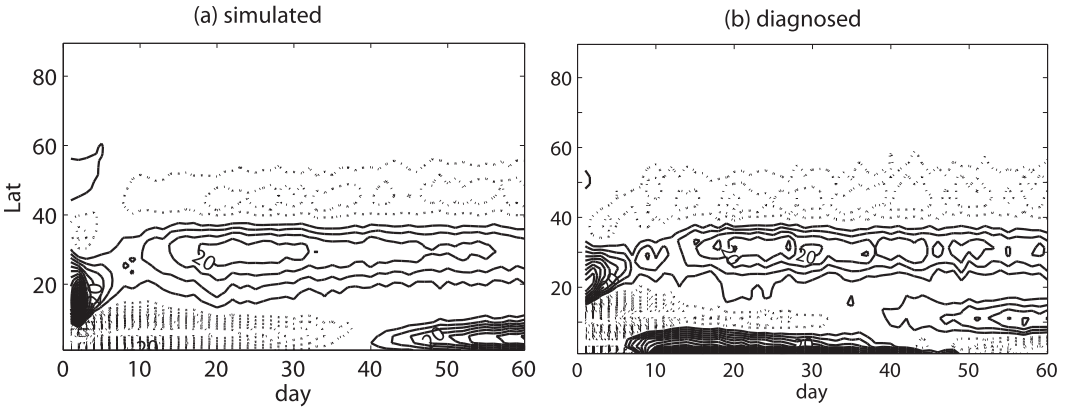

FIG. 7. Zonal and ensemble-mean transient responses of 500-hPa meridional streamfunction (10^9 kg s^{-1}) as a function of latitude and time: (a) simulated as in Fig. 5c and (b) diagnosed from the momentum budget [Eq. (3)].

of 20°. For the subtropical and extratropical changes, the MMC is dominated by the eddy momentum flux divergence, and the zonal wind tendency only plays a minor role in initial several days (not shown). This indicates that the poleward expansion of the Hadley cell edge is primarily driven by the change of eddy momentum flux, while the width of its upward branch is likely controlled by the diabatic heating in the deep tropics. Since the poleward expansions of the Hadley cell edges and midlatitude eddy-driven jets take place earlier than the equatorward contraction of the ITCZ, the Hadley cell expansion is then the consequence of the extratropical eddy momentum forcing rather than the altered diabatic heating in the deep tropics.

b. *The changes of eddy-driven westerly winds projected onto the annular mode*

The fluctuation–dissipation theorem (Leith 1975) suggests that the forced atmospheric changes can be expressed by the leading mode of unforced atmospheric variability, provided that the leading mode is uncorrelated with all other modes. This is arguably the case for the annular modes of the atmosphere that capture a large part of the total variance. Figure 8 shows the leading EOFs of the zonally averaged surface wind, upper-tropospheric zonal wind, and barotropic (i.e., vertically averaged) wind. The zonal wind at each level is weighted by $\cos^{1/2}\phi$ prior to the EOF calculation. As in the observations (e.g., Lorenz and Hartmann 2001), the EOF pattern of zonal wind has a dipolar structure in latitude, and the positive polarity indicates a poleward shift of the eddy-driven jet. Despite the difference in amplitude, the EOFs at different levels share almost the same nodal point at 40° latitude. However, the autocorrelation functions of the corresponding principal components have an unrealistic *e*-folding time longer than 60 days, which is much more persistent than the observations [about 10 days in the Southern Hemisphere in Lorenz and Hartmann (2001)].

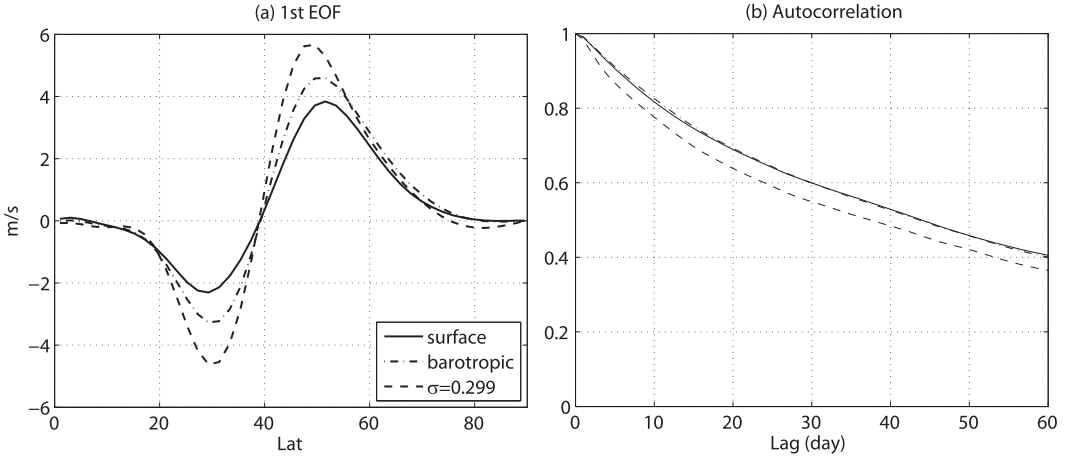

FIG. 8. (a) The leading EOF of zonally averaged surface, barotropic (i.e., vertically averaged), and upper-tropospheric zonal winds and (b) the autocorrelation function of the corresponding principal component (PC). The leading EOF corresponds to one standard deviation of the PC.

Comparing the zonal wind change in Fig. 5 with the leading mode of unforced atmospheric variability at the same level, we notice that the changes of zonal winds resemble the patterns of the unforced annular mode in the middle and lower troposphere, but not in the upper troposphere. Therefore, we focus on the changes of the surface wind rather than the barotropic wind in Lorenz and Hartmann (2001).

In the vertical average of Eq. (2) and ignoring the vertical momentum flux at the surface, the change of surface zonal wind $\overline{u}_s$ can be expressed as

$$\frac{\partial \overline{u}_s}{\partial t} = -\frac{\partial \overline{u}_{\rm tw}}{\partial t} + \left\langle (f+\overline{\zeta})\overline{v} - \overline{\omega}\frac{\partial \overline{u}}{\partial p} \right\rangle - \frac{1}{a\cos^2\phi}\frac{\partial(\langle \overline{v'u'}\rangle \cos^2\phi)}{\partial \phi} - \langle \overline{F}\rangle . \quad (4)$$

Here, the vertical average of X is denoted as $\langle X\rangle = (1/p_s)\int_0^{p_s} X\, dp$, and $\overline{u}_{\rm tw} = \langle \overline{u} - \overline{u}_s\rangle$ is the vertical mean of the zonal wind shear in the thermal wind balance with the meridional temperature gradient. The zonal momentum budget in Eq. (4) can be projected onto the leading EOF of the surface zonal wind:

$$\frac{\partial z_s}{\partial t} = -\frac{\partial z_{\rm tw}}{\partial t} + m_m + m - \frac{z_s}{D}. \quad (5)$$

Here, z_s is the modal projection of the zonally averaged surface zonal wind. In a matrix form, $z_s = u_s \mathbf{W}\mathbf{e}_1/(\mathbf{e}_1^{\rm T}\mathbf{W}\mathbf{e}_1)$, where $\mathbf{e}_1$ is the leading EOF, and $\mathbf{W} = \cos\phi$ is the area weighting. Similarly, $z_{\rm tw}$ is the modal projection of the thermal wind associated with meridional temperature gradient $\overline{u}_{\rm tw}$, and m_m and m are the modal projections of the mean momentum forcing $\langle (f+\overline{\zeta})\overline{v} - \overline{\omega}\partial\overline{u}/\partial p\rangle$ and eddy momentum forcing $-1/(a\cos^2\phi)\partial(\langle \overline{v'u'}\rangle \cos^2\phi)/\partial\phi$. Additionally, the surface friction acting on the annular mode is parameterized by a constant linear damping rate D^{-1} as in Lorenz and Hartmann (2001).

Given the initial condition $[z_s(0) = 0]$, Eq. (5) yields the solution for the ensemble mean annular mode response as a function of time:

$$[z_s(t)] = \int_0^t e^{-(t-s)/D}\mathcal{F}(s)\, ds, \quad \text{where}$$
$$\mathcal{F} = -\frac{\partial [z_{\rm tw}]}{\partial t} + [m_m] + [m], \quad (6)$$

and the square brackets denote the ensemble mean.

The frictional damping rate D^{-1} can be estimated from the control experiment by the low-frequency variability of Eq. (5) (Chen and Plumb 2009). By averaging over segments of 100 days, we have a three-way balance $m_m^{100} + m^{100} = D^{-1}z_s^{100}$, where the superscript 100 denotes an average over 100 days. The least squares fit for the control run yields $D = 5.9$ days, and the change of D from the control run to the perturbed run is less than 5%. This verifies the approximation $\delta z_s/\delta t \ll \delta z_s/D$ for $\delta t = 100$ days. Also, it confirms the general assumption that the change of D with climate change is small such that the change of eddy momentum flux can account for the change of surface westerly winds (e.g., Chen and Held 2007).

Figures 9a and 9c show the total and eddy momentum forcing (i.e., $\mathcal{F}$ and $[m]$) and the predicted annular mode change using Simpson's rule of integration and Eq. (6). The predicted annular mode changes resemble the changes simulated in the model. The changes of surface westerlies are dominated by the eddy momentum flux, and the mean momentum forcing and thermal wind shear change only slightly offset the eddy momentum forcing. As can be seen in Eq. (6), the rate of the adjustment of the annular mode index is controlled by D^{-1}, which itself is derived from the internal variability of the annular mode in the control simulation. Furthermore, if the momentum equation is projected onto the EOF of the barotropic wind, the projection of m^{100} would be smaller for the larger EOF in the barotropic wind (Fig. 8a), and therefore, the estimated $D \approx z^{100}/m^{100}$ would be larger (alternatively, this can be roughly seen without any projection onto a mode by dividing the corresponding zonal wind by momentum flux). As a result, the predicted rate of change in the barotropic wind with a larger D would be slower than the actual simulated rate. Therefore, the numerical calculation suggests the surface westerly wind is more relevant to the analysis of the annular mode change than the barotropic wind.

With the modal projection approach validated above, we now turn our attention to the temporal characteristics of the eddy forcing and feedback. The eddy momentum forcing shows an abrupt increase at about day 6 with slow fluctuations after day 10. Since the 4-K SST warming is turned on instantaneously, the eddy forcing should consist of an abrupt component in response to the initial step-function SST forcing. Further, it is well known that the variability of zonal wind can modify the eddies, which provides a positive eddy feedback to the zonal wind variability (e.g., Robinson 2000; Lorenz and Hartmann 2001). Therefore, following Lorenz and Hartmann (2001), we can parameterize the eddy feedback as a linear function of the annular mode index:

$$m = \tilde{m} + Bz_s, \quad (7)$$

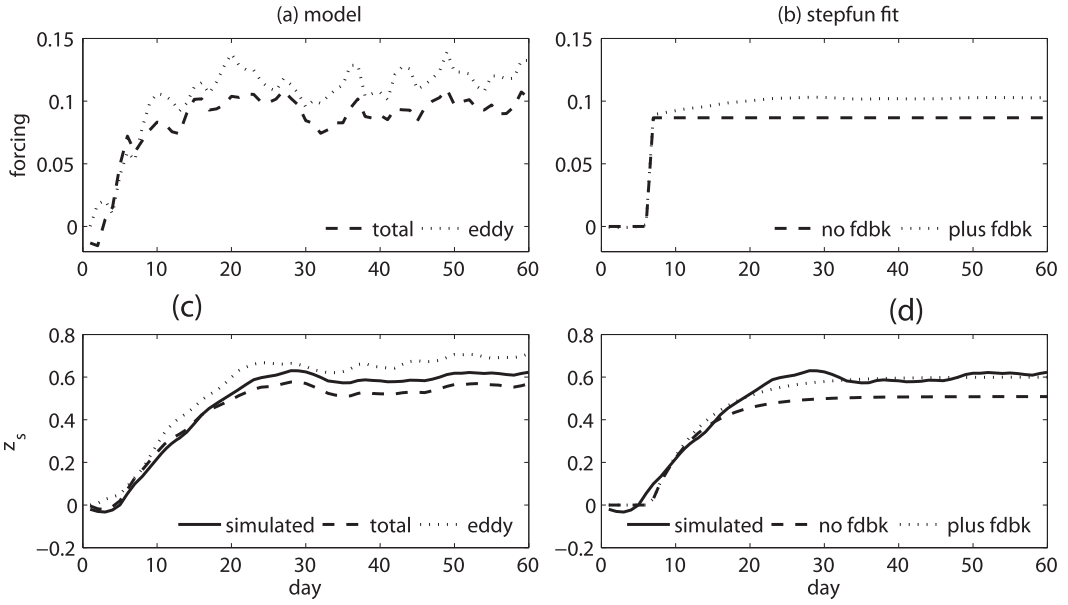

FIG. 9. The projections of momentum forcings and surface winds onto the leading EOF of the unforced variability of surface winds. (a) Total and eddy momentum forcing (day^{-1}), (b) a step-function fit to the total momentum forcing in (a) without and with eddy feedback by minimizing the residual in predicting the simulated wind, (c) the simulated wind in the model and the wind change predicted by the total and eddy momentum forcing in (a), and (d) the surface wind change predicted by the step-function fit in (b) without and with eddy feedback. See the text for details.

where $\tilde{m}$ denotes the eddy forcing due to the initial step-function SST forcing, and B denotes the strength of the feedback. Here, the feedback refers to the reinforcement of the shift of surface westerly wind by the eddies after the surface wind shift has already been initiated.

Substituting Eq. (7) into Eqs. (5) and (6), we have

$$\frac{\partial z_s}{\partial t} = -\frac{\partial z_{\rm tw}}{\partial t} + m_m + m - Bz_s - \frac{z_s}{\tau} \quad \text{and}$$

$$[z_s(t)] = \int_0^t e^{-(t-s)/\tau} \mathcal{F}_{\rm eff}(s)\, ds, \tag{8}$$

where

$$\mathcal{F}_{\rm eff} = \mathcal{F} - B[z_s]. \tag{9}$$

Here, the e-folding time $\tau^{-1} = D^{-1} - B$, and $\mathcal{F}_{\rm eff}$ can be thought of as the effective momentum forcing due to initial SST forcing without the feedback from the changing zonal wind.

We take a simple approach to estimate the strength of eddy feedback in the ensemble transient change by hypothesizing that $\mathcal{F}_{\rm eff}$ can be idealized by a step-function in response to the switch-on SST forcing. We fit the step-function parameters so as to minimize the residual of predicted surface wind change from the simulated wind change. Figures 9b and 9d show the step-function best fit of $\mathcal{F}_{\rm eff}$ and the momentum forcing with feedback $\mathcal{F} = \mathcal{F}_{\rm eff} + B[z_s]$. The best fit of momentum forcings captures the general structure of the simulated momentum forcings. More importantly, in spite of the simplicity of the step-function assumption, the predicted surface wind change with eddy feedback captures the simulated wind change closely, justifying the simple framework.

The fitted momentum forcing also undergoes an abrupt jump in the eddy forcing amplitude after day 6, with a weak positive feedback after the jump. Without the feedback $B = 0$, the zonal index decays exponentially from zero toward the equilibration response with a damping rate of D^{-1}. In the presence of a positive feedback, the rate of change τ^{-1} is slower than D^{-1}, resulting in a larger steady state response. Most of the steady state response in this model setup can be attributable to the response to the effective momentum forcing, and the amplification from the positive feedback is small.

The simple model has limited free parameters: the amplitude and the timing of $\mathcal{F}_{\rm eff}$, D, and τ. In the steady state, the change of the zonal index is related to the effective forcing by $\Delta z_s = \tau \mathcal{F}_{\rm eff}(t = \infty) = (D + BD\tau)\mathcal{F}_{\rm eff}(t = \infty)$. This indicates that the fraction of the zonal index change due to the feedback is $(\tau - D)/\tau = BD$. We can estimate τ with reasonable certainty by the forced response of the zonal index as the e-folding time scale of the unforced variability. Given that τ is close to D, as indicated by Fig. 9d, the contribution of the feedback to the equilibrated change in zonal index BD is small.

Equation (9) can be regarded, to some extent, as an application of the fluctuation–dissipation theorem (Leith 1975) to the zonal momentum budget. However, it appears that the leading mode of the unforced variability of the eddy-driven jet is insufficient to predict the forced annular mode–like response. The dynamical operator τ^{-1} in the perturbed ensemble response differs substantially from the *e*-folding time scale of the unforced annular mode variability (cf. Figs. 8b and 9). Since the frictional damping rate remains almost unchanged, this indicates a large reduction in the eddy feedback from varying zonal flow during the transient response to the SST forcing. When the perturbed run reaches a new equilibrium, the *e*-folding time scale is also smaller than that of the control run, suggesting a covariability between the eddy feedback strength and the eddy-driven jet latitude. One may argue a 4-K uniform SST warming may be too large for the unforced variability to work, but the SST warming ranging from 2 to 5 K (Fig. 3) is within the range of the typical climate sensitivity to a doubling of CO_2. Given that the eddy-driven jet does not seem to be exactly Gaussian as assumed by Leith (1975), a precise application of the fluctuation–dissipation theorem to the annular modes may have to consider a non-Gaussian formulation proposed by Cooper and Haynes (2011).

c. *Cause of the eddy momentum forcing*

The sudden meridional shift in the eddy momentum forcing during days 4–9 is the key to the meridional shifts of the MMC and surface westerly wind, but what causes the momentum flux change? We stress that only through delving into the daily sequence of the adjustment to a step-function-like forcing can one possibly discern the causality of the problem, since the dynamical factors involved can be constantly adjusted toward a statistical equilibrium and a low-frequency average may obscure the causality. Consider the zonal wind changes in the transformed Eulerian mean (TEM) momentum equation (e.g., Edmon et al. 1980; Andrews et al. 1987)

$$\frac{\partial \overline{u}}{\partial t} = f\overline{v}^* + \frac{1}{a\cos\phi}\nabla\cdot\mathbf{F}, \tag{10}$$

where $\overline{v}^*$ is the residual circulation, $\nabla\cdot\mathbf{F}$ is the Eliassen–Palm (EP) flux divergence, and the EP flux $\mathbf{F}$ is the flux of wave activity. In the QG limit, the EP flux divergence is also equal to the PV flux

$$\frac{1}{a\cos\phi}\nabla\cdot\mathbf{F} = \overline{v'q'} = -\frac{1}{a\cos^2\phi}\frac{\partial(\overline{v'u'}\cos^2\phi)}{\partial\phi} + \frac{\partial}{\partial p}\left(\frac{f\overline{v'\theta'}}{\partial\tilde{\theta}/\partial p}\right). \tag{11}$$

Here, the QG PV is $q = f + \zeta + f(\partial/\partial p)\{(\theta - \tilde{\theta})/(\partial\tilde{\theta}/\partial p)\}$; $\tilde{\theta}$ is the hemispheric mean potential temperature at each pressure level.

Figure 10 shows the EP cross section for the climatology and the changes during different stages of the transient adjustment. In the time mean, the EP vectors show the familiar pattern of upward and equatorward wave propagation as in the observations (Edmon et al. 1980). There are two notable regions of EP flux convergence: one in the middle troposphere to the poleward side of the jet associated with upward wave activity flux, and the other in the upper troposphere on the jet's equatorward flank associated with equatorward wave activity flux. The momentum flux convergence (red contours) coincides with the jet center, where it is largely balanced by the vertical component of EP flux convergence. As such, the jet core coincides with a PV flux minimum, where irreversible eddy mixing is weak and the nonacceleration theorem of Charney and Drazin (1961) may apply.

After the SST warming is turned on, the upward wave activity flux increases substantially during the first 4 days, likely owing to the sudden reduction of static stability induced by surface warming and the resultant increase of baroclinic instability (Fig. 6a). The upward wave activity flux gives rise to increased momentum convergence at the jet core, which can be roughly thought of as an enhancement of the mean momentum flux due to more vigorous eddies. The upward wave activity flux in the lower troposphere starts to decrease after the first few days, likely resulting from increased lower-level static stability. From days 4 to 9, there is pronounced anomalous EP flux divergence at 300–500 hPa and 40°–50°, associated with anomalous upward wave activity flux above this region and downward wave activity flux below this (Fig. 10c). We stress that this anomalous divergence does not arise from an increase in the lower-level baroclinicity but less dissipation in this region, as evidenced by the reduction of the upward EP flux from the lower level. As this anomalous divergence is located on the poleward flank of the jet, it leads to a poleward shift of the eddy momentum forcing and consequently eddy-driven circulation. After day 9, the eddies start to weaken the mean momentum flux, which may be traced to a reduction of the lower-level baroclinicity associated with increased static stability. This projects weakly onto the shift of the eddy forcing, which is consistent with the weak zonal index feedback revealed from the modal projection analysis in section 4b. The change after day 9 is roughly the mirror image of the change during days 1–4 (cf. Figs. 10b,d), which can be thought of as a slow recovery after an immediate reaction to a large instantaneous SST warming.

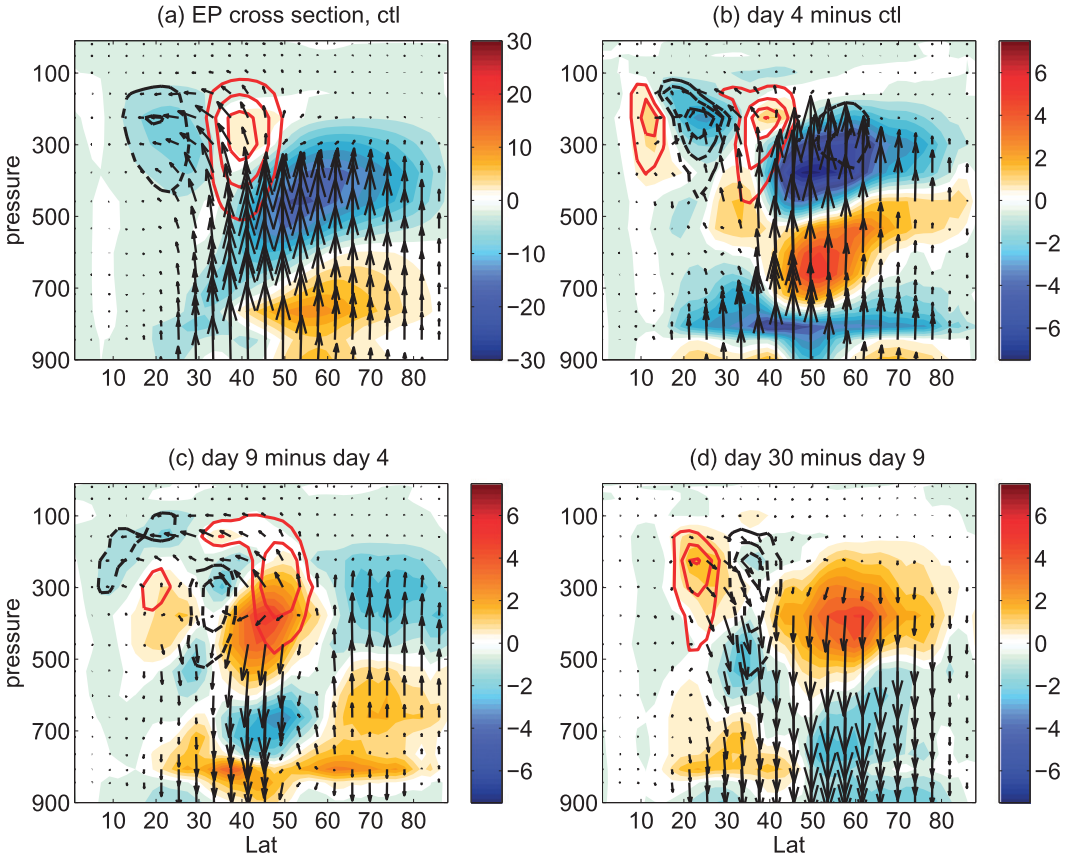

FIG. 10. The EP cross section for (a) the climatology, (b) day 4 minus climatology, (c) day 9 minus day 4, and (d) day 30 minus day 9. The shading denotes the eddy EP flux divergence ($\mathrm{m\,s^{-1}\,day^{-1}}$), the arrows denote the EP vectors, and the contours denote the eddy momentum flux convergence [red for convergence and black for divergence; interval: $2\,\mathrm{m\,s^{-1}\,day^{-1}}$ for (a), $0.5\,\mathrm{m\,s^{-1}\,day^{-1}}$ for (b),(c), and (d)].

The change of EP flux divergence can be further explicated by considering the wave activity budget. The wave activity for small-amplitude waves can be defined as $A = (0.5a)\overline{q'^2}/(\partial\overline{q}/\partial\phi)$, where $(1/a)\partial\overline{q}/\partial\phi$ is the Eulerian PV gradient. However, the direct application of this definition is very limited, since $\partial\overline{q}/\partial\phi$ in the realistic turbulent flow can reverse its sign during wave breaking events, leading to singularity in A.

Recently, using the concept of the equivalent latitude (Butchart and Remsberg 1986), Nakamura and Solomon (2010) introduced a modified definition for wave activity that holds for both linear small-amplitude and nonlinear finite-amplitude eddies. Considering the PV as a quasi-conservative tracer, the equivalent latitude ϕ_e for the PV value Q is determined by the requirement that the areas covered by the following two integrals are equal:

$$\iint_{Q\le q(\phi'),\phi'\le\pi/2} dS = \iint_{\phi_e\le\phi'\le\pi/2} dS = 2\pi a^2(1-\sin\phi_e). \tag{12}$$

Here, the area element is $dS = a^2\cos\phi' d\lambda d\phi'$. Using a simple box counting method, Eq. (12) yields a monotonic relationship between Q and ϕ_e, which can be inverted as $Q(\phi_e)$. Given the PV conservation, $Q(\phi_e)$ is also a material surface, and therefore Q denotes the Lagrangian PV that is conserved in the absence of dissipation and diabatic heating. As such, $(1/a)\partial Q/\partial\phi_e$ can be referred to as the Lagrangian PV gradient, and this eliminates the singularity in the Eulerian PV gradient. Nakamura and Solomon (2010) defined the wave activity at the equivalent latitude ϕ_e as

$$A(\phi_e) = \frac{1}{2\pi a\cos\phi_e}\left\{\iint_{Q(\phi_e)\le q(\phi'),\phi'\le\pi/2} q\,dS - \iint_{\phi_e\le\phi'\le\pi/2} q\,dS\right\}, \tag{13}$$

which measures the net displacement of PV contours from zonal symmetry and reduces to the familiar form of

pseudomomentum $(0.5a)\overline{q'^2}/(\partial\overline{q}/\partial\phi)$ for the small-amplitude limit [see appendix A in Nakamura and Zhu (2010) for details].

Taking time derivative of Eq. (13) yields a pseudomomentum constraint for the PV flux [see the derivations for Eq. (30) in Nakamura and Zhu (2010)]:

$$\overline{v'q'} \approx -\frac{\partial A(\phi_e)}{\partial t} - \kappa_{\rm eff}(\phi_e, t)\frac{1}{a}\frac{\partial Q(\phi_e, t)}{\partial \phi_e}, \qquad (14)$$

where $\kappa_{\rm eff}$ is the effective diffusivity of the irreversible horizontal mixing of PV across material surfaces (e.g., Nakamura 1996). Roughly speaking, the effective diffusivity is related to the length of PV contours. Within the vicinity of strong PV mixing, the PV contours are complex and the diffusivity is then large. By contrast, the PV gradient would be conserved for reversible processes, and an example of this is illustrated in Fig. 1 of Nakamura (1996).

One may wonder why the Lagrangian PV gradient is used for the eddy diffusive closure rather than the Eulerian counterpart. Taking the derivative of Eq. (13) with respect to the latitude, one obtains a simple relationship between the Eulerian and Lagrangian PV gradients (Nakamura and Zhu 2010):

$$\frac{\partial\overline{q}}{\partial\phi} - \frac{\partial Q}{\partial\phi_e} = \frac{\partial}{\partial\phi_e}\left\{\frac{1}{a\cos\phi_e}\frac{\partial(A\cos\phi_e)}{\partial\phi_e}\right\}. \qquad (15)$$

If the eddy amplitude is zero, the Eulerian and Lagrangian PV gradients are identical. In the surf zone where the PV is efficiently mixed, the Eulerian PV gradient is close to zero and the diffusivity can be ill posed. The Lagrangian PV gradient is, however, positive definite, and therefore the corresponding eddy diffusivity is well posed.

In the conservative (i.e., adiabatic and frictionless) limit, the PV flux is opposite to the rate of change in wave activity, and the PV flux is zero in steady state [i.e., the finite-amplitude extension of the nonacceleration theorem of Charney and Drazin (1961) in the QG framework]. This is often not satisfied for the Eulerian diagnostics of finite-amplitude eddies because of a cubic eddy term that can be ignored only for small-amplitude eddies [see the discussion in section 2a of Nakamura and Zhu (2010)]. It is important to note that this is a hybrid Eulerian–Lagrangian diagnostics: the eddy flux is local in latitude, but the wave activity and Lagrangian PV gradient are evaluated following the material surfaces of PV contours. The Eulerian and Lagrangian diagnostics are connected by setting the equivalent latitude in A and Q equal to the latitude in $\overline{v'q'}$.

We diagnose the eddy flux and wave activity directly from the model output, and estimate the effective diffusivity indirectly as the residual in Eq. (14). Note that the diabatic heating in the budget has been ignored, and thus we only examine the budget for the upper troposphere (above 500 hPa), where the diabatic heating is arguably smaller than the terms retained except at the jet core.[2] Caution should also be used in interpreting the results within the deep tropics as the QG approximation is no longer valid.

The upper-tropospheric pseudomomentum budget is shown in Fig. 11. In the steady state, the PV flux is balanced by the dissipation due to the PV mixing as indicated by Eq. (14). The dissipation in black contours identifies two primary regions of irreversible mixing (or wave sinks): one located at the jet's poleward side confined between the tropopause and the steering level, the other on the jet's equatorward flank corresponding to the subtropical critical latitudes. The changes of the terms in Eq. (14) from days 4 to 9 are broken down and displayed in shading. It is clear that the appearance of the anomalous PV flux (or EP flux divergence) at 300–500 hPa and 40°–50° mainly results from the change of eddy dissipation of pseudomomentum. The change of the wave activity tendency appears to be in quadrature with and thus contributes little to the PV flux change. The dissipation change in that region can be further decomposed into the change of effective diffusivity and that of PV gradient. While the effect of changing diffusivity has a greater magnitude than altered PV gradient, the effect of diffusivity change is relatively uniform at the jet core and thus is not a major contributor to the momentum flux shift in latitude (cf. Figs. 10c and 11e).

While the dissipation change due to effective diffusivity alone has a small projection onto the jet shift, it plays a critical role in shaping the PV gradient. Ignoring slow thermal damping in Eq. (48) of Nakamura and Zhu (2010), the rapid change in the Lagrangian PV gradient can be expressed as a diffusive equation:

$$\frac{\partial}{\partial t}\left(\frac{\partial Q}{\partial\phi_e}\right) \approx \frac{1}{a^2}\frac{\partial}{\partial\phi_e}\left\{\frac{1}{\cos\phi_e}\frac{\partial}{\partial\phi_e}\left(\kappa_{\rm eff}\cos\phi_e\frac{\partial Q}{\partial\phi_e}\right)\right\}. \qquad (16)$$

This indicates an increase in diffusivity reduces the local Lagrangian PV gradient. Indeed, Figs. 11f and 11g show

[2] The climatological-mean countergradient PV flux at the jet core in Fig. 11a seems to disagree with Eq. (14). This can be attributed to that Eq. (14) ignores the diabatic heating term in Eq. (24a) of Nakamura and Zhu (2010). Plate 5 of Haynes and Shuckburgh (2000) showed the effective diffusivity is very small at the jet core (i.e., a mixing barrier), where the diabatic term can be equally important.

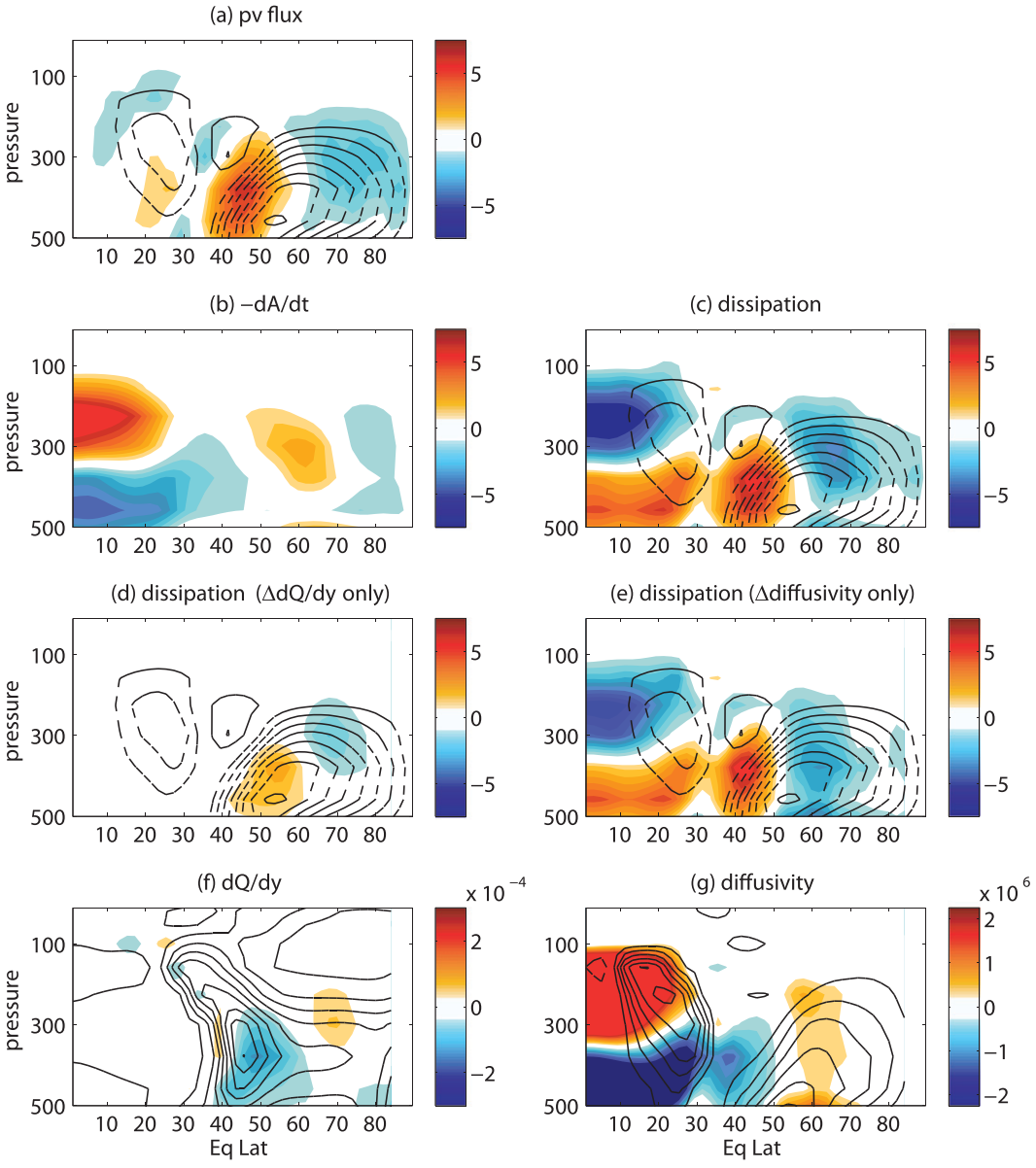

FIG. 11. The zonal and ensemble-mean change of the pseudomomentum budget [Eq. (14)] from days 4 to 9. (a) Eddy PV flux change, (b) negative wave activity tendency change, (c) total eddy dissipation change, (d) dissipation change due to PV gradient change, (e) dissipation change due to effective diffusivity change, (f) PV gradient change, and (g) effective diffusivity change. The contours in (a)–(e) are the climatological-mean PV flux (equal to dissipation) with contour interval of $2\,\mathrm{m\,s^{-1}\,day^{-1}}$. The contours in (f) and (g) are climatological-mean $\partial Q/\partial\phi_e$ (interval of $8 \times 10^{-5}\,\mathrm{s^{-1}}$) and κ_{eff} (interval of $0.6 \times 10^{6}\,\mathrm{m^2\,s^{-1}}$). Note that the plot is shown above 500 hPa.

that there is an increase in effective diffusivity on the jet's poleward flank where mixing is strong and a reduction within the jet core where mixing is weak. The sharpened meridional gradient in effective diffusivity from 40° to 60° is consistent with the reduction in the Lagrangian PV gradient. This self-consistency is not surprising since the diffusivity is inferred as a residual. It would be interesting to link the diffusivity change to more physically based wave breaking and the processes leading up to the breaking events, although a detailed analysis is beyond the scope of this study.

Substituting Eq. (11) into Eq. (14) and taking the upper-tropospheric average, the eddy momentum flux convergence is equal to the sum of the negative rate of change in wave activity, the convergence of upward wave activity flux, and the dissipation due to effective diffusion

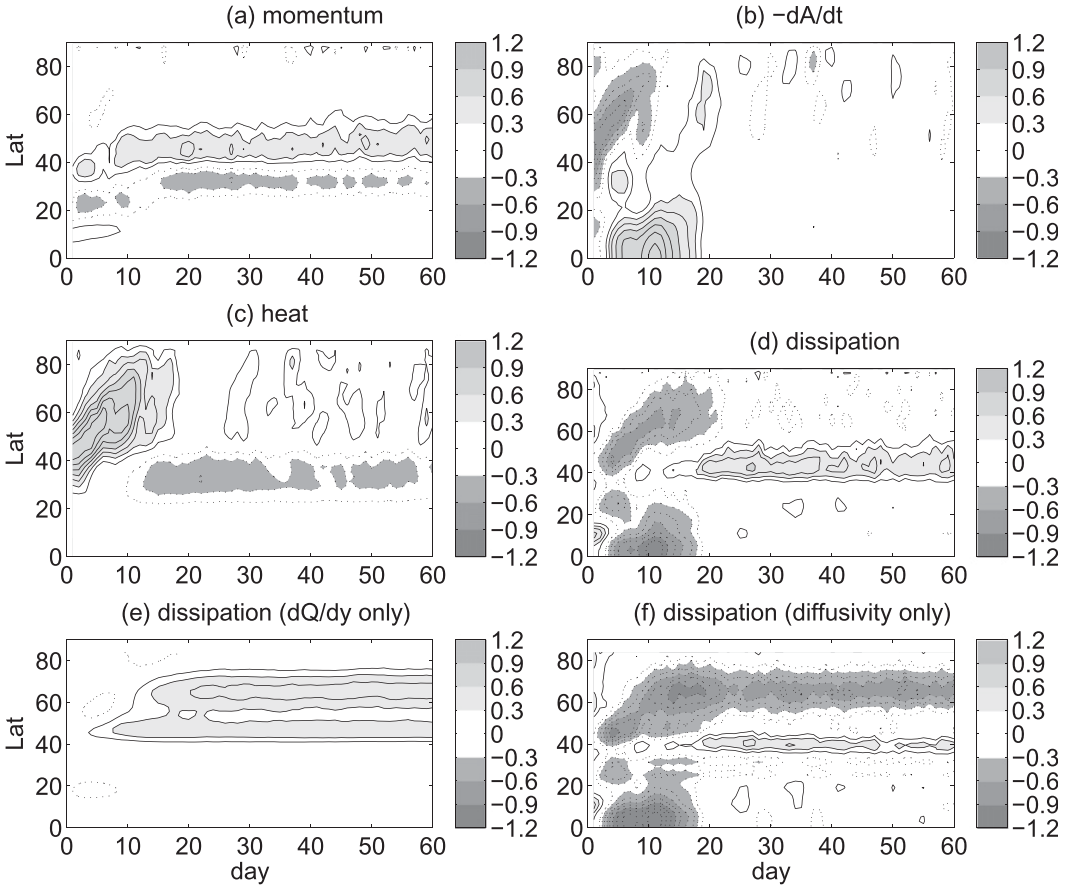

FIG. 12. The zonal and ensemble-mean transient responses of the upper-tropospheric (0–500 hPa) average of the pseudomomentum budget [Eq. (17); $\mathrm{m\,s^{-1}\,day^{-1}}$] as a function of latitude and time. (a) Eddy momentum flux convergence, (b) negative wave activity tendency, (c) vertical EP flux divergence, (d) total eddy dissipation, (e) dissipation change due to PV gradient change, and (f) dissipation change due to effective diffusivity change.

in the upper troposphere. This provides a dynamical framework to diagnose the cause of eddy momentum flux change on a day-to-day basis:

$$-\frac{1}{a\cos^2\phi}\frac{\partial(\langle\overline{v'u'}\rangle_U\cos^2\phi)}{\partial\phi}=-\frac{\partial\langle A\rangle_U}{\partial t}-\frac{1}{p_{500}}\left(\frac{f\overline{v'\theta'}}{\partial\tilde{\theta}/\partial p}\right)\Bigg|_{500\mathrm{hPa}}-\left\langle\kappa_{\mathrm{eff}}\frac{1}{a}\frac{\partial Q}{\partial\phi_e}\right\rangle_U. \quad (17)$$

Figures 12a–d delineate the budget above (i.e., Fig. 12a = Fig 12b + Fig. 12c + Fig. 12d) as a function of latitude and time. During days 1–4, the momentum flux convergence increases at the jet center, largely because of the increased wave activity flux convergence from the lower level (see also Fig. 10). Next, during days 5–9, the momentum convergence increases between the latitudes 40° and 50°, and this increase and its sharpness can be explained by the rapid reduction (i.e., a transition from negative to positive anomalies) in eddy dissipation (Fig. 12d). Although the vertical EP flux convergence has a same-signed anomaly as the momentum flux convergence during the same period, the vertical component seems to only participate in, but not instigate, the sharp transition. In steady state, the reduced dissipation accounts for the momentum convergence on the jet's poleward flank and the reduced upward wave activity flux for the divergence on the equatorward flank—the latter consistent with previous idealized studies (e.g., Lu et al. 2010; Butler et al. 2011).

As far as the wave activity tendency is concerned, it can be regarded as a communicator between the lower-tropospheric baroclinicity and upper-tropospheric PV mixing, since it is large in the initial adjustment and vanishes in the equilibrium. One may argue that the increase in the upward wave activity flux gives rise to a positive wave activity tendency in the upper level, as the baroclinic waves propagate from the lower level into

the upper level. The larger wave activity in the upper level, in turn, leads to an enhancement in the eddy dissipation as a result of more vigorous PV mixing in the surf zone. Regardless of the fluctuations in wave activity, we stress that only through modifying the irreversible mixing can the wave activity affect the time-mean PV flux, as expected from Eq. (14).

The dissipation change is further decomposed into the change due to the PV gradient and that due to the effective diffusivity (Figs. 12e,f). The figure suggests that the reduction in dissipation associated with the weakened midlatitude PV gradient contributes most to the low-frequency change in the momentum forcing, whereas the change in effective diffusivity accounts for most of the eddy dissipation change. In the steady state, the latter effect only enhances the dissipation everywhere in the extratropics except near the jet center, thus contributing little to the maintenance of the circulation shift, although it plays a critical role in shaping the PV gradient change.

The individual contributions to the momentum forcing can be further elucidated by projecting the upper-tropospheric averages onto the annular mode pattern. Figure 13 (top) shows that much of the wave activity tendency can be accounted for by the vertical EP flux convergence into the upper troposphere and that the cancelation between the two gives rise to a small net effect on the momentum flux shift. By contrast, the jump in the eddy momentum forcing during days 4–9 is due to the dissipation change during this period, consistent with Fig. 11. Furthermore, as the dissipation change is divided between the diffusivity and PV gradient changes (Fig. 13, bottom), most of the momentum flux change is attributable to the dissipation change due to the altered Lagrangian mean PV gradient. The combined effect of heat flux convergence and changing effective diffusivity is used to produce the wave activity tendency, and the net effect of the three on the momentum flux shift is nearly zero. This epitomizes the role of the wave activity in exchanging pseudomomentum reversibly between the lower-level baroclinicity and upper-level mixing. This three-way cancelation emphasizes that the irreversible change in the Lagrangian PV gradient is the most essential element in the shift of the eddy-driven circulation.

One may argue that the change of the Lagrangian PV gradient is itself caused by the shift of a Eulerian jet or Eulerian PV gradient. However, in the conservative limit, the Lagrangian PV gradient remains constant, and the Eulerian PV gradient change cancels with the wave activity change in Eq. (15). Therefore, the Lagrangian PV gradient cannot be predicted by the Eulerian gradient, which can be largely canceled by the eddy change. More importantly, the change of the Lagrangian PV gradient can be predicted by Eq. (16) with the distribution of eddy

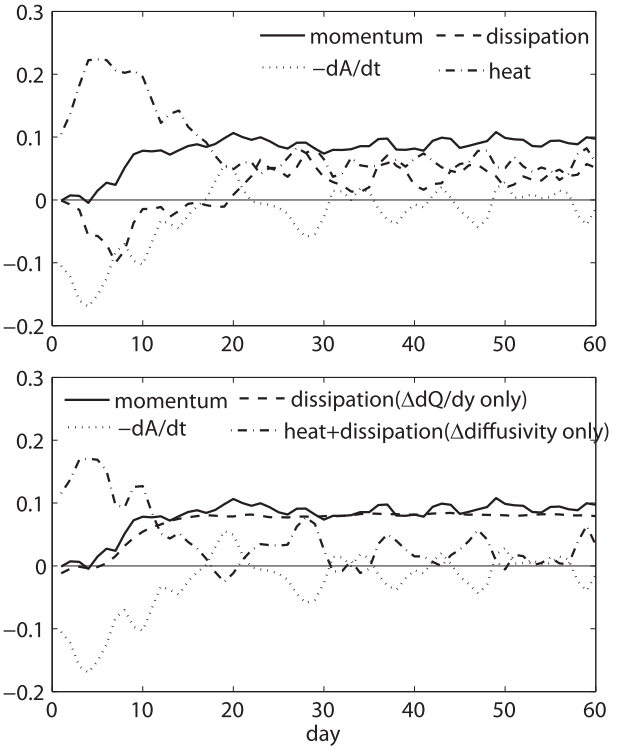

FIG. 13. The projections of the upper-tropospheric average of the pseudomomentum budget (Fig. 12; day^{-1}) onto the annular mode. (top) Momentum convergence = dissipation + $(-dA/dt)$ + vertical EP flux divergence. (bottom) Momentum convergence = dissipation due to PV gradient change + $(-dA/dt)$ + (vertical EP flux divergence + dissipation due to diffusivity change).

diffusivity. The eddy diffusivity is a character of the circulation, and it can be obtained with either PV or a passive tracer (e.g., Haynes and Shuckburgh 2000).

Here, we recapitulate the key processes that lead up to the poleward shift of the MMC and eddy-driven jet in response to an instantaneous uniform SST warming:

- Stage 1—days 1–4: With an abrupt switch on of a uniform SST warming, the atmosphere becomes more unstable and generates more vigorous baroclinic waves, enhancing upper-tropospheric eddy mixing and converging momentum flux into the mean jet.
- Stage 2—days 4–9: The enhancement in mixing reduce the Lagrangian PV gradient on the jet's poleward flank where the effective diffusivity is large, leading to a local reduction of the pseudomomentum dissipation (positive trend meaning reduction in Fig. 10). This reduction allows more waves to survive the dissipation and propagate away from the latitudes of baroclinic generation on the jet's poleward flank. This equatorward propagation gives rise to a poleward shift in the momentum forcing and constitutes the onset of a step-function-like effective momentum forcing for the annular mode.

- Stage 3—after day 9: With a simple parameterization of the eddy feedback from the zonal flow, the annular mode responds to the effective forcing in a manner reminiscent of the transient adjustment in a forced dissipative system. However, the decay rate is much faster than that of the unforced annular mode variability, arguably resulting from the reduced eddy feedback in a changing zonal flow.

5. Discussion

We now discuss different mechanisms for the circulation shift in the context of our large-ensemble transient experiment and new diagnostic framework. Using the pseudomomentum budget, we obtain Eq. (17), wherein the eddy momentum flux can be attributed to the wave activity tendency, convergence of upward wave activity flux, and eddy dissipation in the upper troposphere. Provided that the momentum flux is known, the surface westerlies can be determined through the vertically averaged momentum budget. Our method refines the eddy diffusive closure made in Butler et al. (2011) in support of the importance of isentropic slope, which dominates the Lagrangian PV gradient. The time-dependent eddy PV fluxes are not necessarily downgradient, owing to the altered wave activity [see Eq. (14)]. Also, both the climatological mean and the change of effective diffusivity have sophisticated spatial structure (Fig. 11g), whereas Butler et al. (2011) assumed no change in eddy diffusivity.

Projecting the momentum equation onto the annular mode pattern, one can construct a forced-dissipative system for the transient adjustment of the annular mode, whereby the cause for the annular mode–like response to an external forcing can be detected. This approach identifies that the onset of the shift in the momentum forcing results mainly from a reduction in eddy dissipation in the upper troposphere. In contrast, the eddy heat flux previously deemed important in equilibrium (Lu et al. 2010) and in a transient dynamical response (Butler et al. 2011) is largely canceled by the wave activity tendency, and does not contribute directly to the abrupt shift in latitude in the momentum forcing. Therefore, while the latitudinal shift of lower-level baroclinicity can help to maintain the shift of the eddy-driven jet in the equilibrium through a baroclinic eddy feedback (e.g., Robinson 2000), causality may not be assigned for the initial jet shift.

We argue that the Lagrangian PV gradient from Eq. (15) is dynamically more relevant than the Eulerian PV gradient for finite-amplitude eddies, since under strong mixing, an eddy diffusive closure based on a near-zero Eulerian gradient can be ill posed. By following the quasi-conservative PV surface, the Lagrangian PV gradient can be altered only through dissipative or diabatic processes, whereas the Eulerian gradient can be also modified by the high-order terms that can be ignored only for small-amplitude eddies (Nakamura and Zhu 2010). Similar benefits have been widely recognized in the diagnostic of the mixing at the polar vortex where the Lagrangian mean can better characterize the boundary of the vortex than the Eulerian mean (Butchart and Remsberg 1986). A recent study by Solomon et al. (2012) found the Lagrangian PV gradient is better at predicting the type of baroclinic eddy life cycle than the Eulerian PV gradient, partly because the Eulerian PV gradient at the surf zone is largely homogenized. The Lagrangian method also highlights the distinction between irreversible versus reversible processes. For example, Eq. (17) shows wave propagation alone (i.e., transient fluctuations in A) with fixed lower-level baroclinicity cannot modify eddy momentum flux in the steady state unless the propagation leads to irreversible wave breaking or absorption (i.e., the change of $\kappa_{\rm eff}$ or $\partial Q/\partial\phi_e$).

Similar to our result, Barnes and Hartmann (2010) and Kidston and Vallis (2012) stressed a reduction in dissipation on the poleward flank of the jet under climate warming. They further argued that it can be explained by a transition from an absorbing critical latitude to a reflecting turning latitude, resulting in additional momentum convergence on the jet's poleward flank. Our result, however, shows that the region (300–500 hPa, 40–50°) of reduced dissipation exhibits almost no poleward wave propagation in the climatology mean (cf. Figs. 10a and 10c), and therefore the momentum convergence on the jet's poleward flank is associated with increased vertical wave propagation rather than reduced poleward wave propagation. Our interpretation is also consistent with diagnosis of wave breaking frequency with climate warming in Rivière (2011), who found increased frequency of anticyclonic wave breaking on the equatorward flank of the jet and little change in the cyclonic wave breaking on the poleward flank.

6. Summary

The atmospheric response to an instantaneous uniform SST warming on an idealized aquaplanet model is investigated as an example to understand the eddy–zonal flow interaction under climate change. A large ensemble of transient experiments show a fast poleward shift of the midlatitude eddy-driven winds and the edge of the Hadley cell and a slow equatorward contraction of the upward branch of the Hadley cell and ITCZ. Different timings of hydrological cycle changes suggest that the subtropical drying and midlatitude shift in

precipitation are due to the midlatitude circulation shifts rather than the direct response to the altered heating in the deep tropics.

The extratropical circulation changes are analyzed from the perspective of the annular mode by means of projecting the momentum equation and finite-amplitude pseudomomentum budget onto the annular mode pattern. The result suggests that the shift of the edge of the Hadley cell and the eddy-driven jet can be interpreted as an annular mode–like response to a sudden onset of a step-function-like momentum forcing plus a simple parameterization of the eddy feedback from the zonal flow. The rather weak eddy feedback compared to that in the unforced annular mode variability suggests that a precise application of the fluctuation–dissipation theorem (Leith 1975) to the annular mode may have to consider its possible interactions with other modes or the non-Gaussianity in the annular mode (e.g., Cooper and Haynes 2011). One may argue a 4-K uniform SST warming may be too large for the unforced variability to work precisely. However, the SST warming ranging from 2 to 5 K (Fig. 3) is within the range of the typical climate sensitivity to a doubling of CO_2.

Our results shed light on the causality of the circulation shift in a warmer climate: the poleward movement of eddy momentum flux and the eddy-driven circulation can be attributed to a reduced midtropospheric Lagrangian PV gradient. As a result, the downgradient PV flux is reduced, leading to more upward and equatorward wave propagation away from the regions of baroclinic generation. While it remains to apply our diagnostics to a wide range of climate regimes (e.g., Lu et al. 2010) or an instantaneous doubling of CO_2 (Wu et al. 2011), our results underline the importance of irreversible processes, particularly those related to the mixing of the Lagrangian PV gradient under climate change.

Acknowledgments. We benefited considerably from the discussions with Alan Plumb, Ari Solomon, and Walt Robinson. We are grateful to anonymous reviewers and editor Ming Cai for comments and suggestions, and to Noboru Nakamura for a careful review of our manuscript that helped tighten the relationship between the Lagrangian PV gradient and effective diffusivity changes. GC is supported by NSF Grant AGS-1064079, and JL is supported by NSF Grant AGS-1064045. GC and LS are also partially supported by a startup fund at Cornell University.

REFERENCES

Andrews, D. G., J. R. Holton, and C. B. Leovy, 1987: *Middle Atmosphere Dynamics.* Academic Press, 489 pp.

Barnes, E. A., and D. L. Hartmann, 2010: Testing a theory for the effect of latitude on the persistence of eddy-driven jets using CMIP3 simulations. *Geophys. Res. Lett.,* **37,** L15801, doi:10.1029/2010GL044144.

——, ——, D. M. W. Frierson, and J. Kidston, 2010: Effect of latitude on the persistence of eddy-driven jets. *Geophys. Res. Lett.,* **37,** L11804, doi:10.1029/2010GL043199.

Brayshaw, D. J., B. J. Hoskins, and M. Blackburn, 2008: The storm-track response to idealized SST perturbations in an aqua-planet GCM. *J. Atmos. Sci.,* **65,** 2842–2860.

Butchart, N., and E. E. Remsberg, 1986: The area of the stratospheric polar vortex as a diagnostic for tracer transport on an isentropic surface. *J. Atmos. Sci.,* **43,** 1319–1339.

Butler, A. H., D. W. J. Thompson, and T. Birner, 2011: Isentropic slopes, downgradient eddy fluxes, and the extratropical atmospheric circulation response to tropical tropospheric heating. *J. Atmos. Sci.,* **68,** 2292–2305.

Caballero, R., 2005: The dynamic range of poleward energy transport in an atmospheric general circulation model. *Geophys. Res. Lett.,* **32,** L02705, doi:10.1029/2004GL021581.

Cai, M., and K.-K. Tung, 2012: Robustness of dynamical feedbacks from radiative forcing: 2% solar versus 2 × CO_2 experiments in an idealized GCM. *J. Atmos. Sci.,* **69,** 2256–2271.

Charney, J. G., and P. G. Drazin, 1961: Propagation of planetary-scale disturbances from the lower into the upper atmosphere. *J. Geophys. Res.,* **66,** 83–109.

Chen, G., and I. M. Held, 2007: Phase speed spectra and the recent poleward shift of Southern Hemisphere surface westerlies. *Geophys. Res. Lett.,* **34,** L21805, doi:10.1029/2007GL031200.

——, and R. A. Plumb, 2009: Quantifying the eddy feedback and the persistence of the zonal index in an idealized atmospheric model. *J. Atmos. Sci.,* **66,** 3707–3720.

——, I. M. Held, and W. A. Robinson, 2007: Sensitivity of the latitude of the surface westerlies to surface friction. *J. Atmos. Sci.,* **64,** 2899–2915.

——, J. Lu, and D. M. W. Frierson, 2008: Phase speed spectra and the latitude of surface westerlies: Interannual variability and global warming trend. *J. Climate,* **21,** 5942–5959.

——, R. A. Plumb, and J. Lu, 2010: Sensitivities of zonal mean atmospheric circulation to SST warming in an aqua-planet model. *Geophys. Res. Lett.,* **37,** L12701, doi:10.1029/2010GL043473.

Cooper, F. C., and P. H. Haynes, 2011: Climate sensitivity via a nonparametric fluctuation–dissipation theorem. *J. Atmos. Sci.,* **68,** 937–953.

Delworth, T. L., and Coauthors, 2006: GFDL's CM2 global coupled climate models. Part I: Formulation and simulation characteristics. *J. Climate,* **19,** 643–674.

Edmon, H. J., B. J. Hoskins, and M. E. McIntyre, 1980: Eliassen–Palm cross sections for the troposphere. *J. Atmos. Sci.,* **37,** 2600–2616.

Frierson, D. M. W., 2006: Robust increases in midlatitude static stability in simulations of global warming. *Geophys. Res. Lett.,* **33,** L24816, doi:10.1029/2006GL027504.

——, I. M. Held, and P. Zurita-Gotor, 2006: A gray-radiation aquaplanet moist GCM. Part I: Static stability and eddy scale. *J. Atmos. Sci.,* **63,** 2548–2566.

——, J. Lu, and G. Chen, 2007: Width of the Hadley cell in simple and comprehensive general circulation models. *Geophys. Res. Lett.,* **34,** L18804, doi:10.1029/2007GL031115.

Gerber, E. P., S. Voronin, and L. M. Polvani, 2008: Testing the annular mode autocorrelation time scale in simple atmospheric general circulation models. *Mon. Wea. Rev.,* **136,** 1523–1536.

Haynes, P. H., and E. F. Shuckburgh, 2000: Effective diffusivity as a diagnostic of atmospheric transport: 1. Stratosphere. *J. Geophys. Res.,* **105** (D18), 22 795–22 810.

Held, I. M., and A. Y. Hou, 1980: Nonlinear axially symmetric circulations in a nearly inviscid atmosphere. *J. Atmos. Sci.,* **37,** 515–533.

——, and B. J. Soden, 2006: Robust responses of the hydrological cycle to global warming. *J. Climate,* **19,** 5686–5699.

Joseph, R., M. Ting, and P. J. Kushner, 2004: The global stationary wave response to climate change in a coupled GCM. *J. Climate,* **17,** 540–556.

Kidston, J., and E. P. Gerber, 2010: Intermodel variability of the poleward shift of the austral jet stream in the CMIP3 integrations linked to biases in 20th century climatology. *Geophys. Res. Lett.,* **37,** L09708, doi:10.1029/2010GL042873.

——, and G. K. Vallis, 2012: The relationship between the speed and the latitude of an eddy-driven jet in a stirred barotropic model. *J. Atmos. Sci.,* **69,** 3251–3263.

——, ——, S. M. Dean, and J. A. Renwick, 2011: Can the increase in the eddy length scale under global warming cause the poleward shift of the jet streams? *J. Climate,* **24,** 3764–3780.

Kodama, C., and T. Iwasaki, 2009: Influence of the SST rise on baroclinic instability wave activity under an aquaplanet condition. *J. Atmos. Sci.,* **66,** 2272–2287.

Korty, R. L., and T. Schneider, 2008: Extent of Hadley circulations in dry atmospheres. *Geophys. Res. Lett.,* **35,** L23803, doi:10.1029/2008GL035847.

Leith, C., 1975: Climate response and fluctuation dissipation. *J. Atmos. Sci.,* **32,** 2022–2026.

Lorenz, D. J., and D. L. Hartmann, 2001: Eddy–zonal flow feedback in the Southern Hemisphere. *J. Atmos. Sci.,* **58,** 3312–3327.

——, and E. T. DeWeaver, 2007a: The response of the extratropical hydrological cycle to global warming. *J. Climate,* **20,** 3470–3484.

——, and ——, 2007b: Tropopause height and zonal wind response to global warming in the IPCC scenario integrations. *J. Geophys. Res.,* **112,** D10119, doi:10.1029/2006JD008087.

Lu, J., and B. Zhao, 2012: The oceanic feedback in the climate response to doubling CO_2. *J. Climate,* **25,** 7544–7563.

——, G. A. Vecchi, and T. Reichler, 2007: Expansion of the Hadley cell under global warming. *Geophys. Res. Lett.,* **34,** L06805, doi:10.1029/2006GL028443.

——, G. Chen, and D. M. W. Frierson, 2008: Response of the zonal mean atmospheric circulation to El Niño versus global warming. *J. Climate,* **21,** 5835–5851.

——, ——, and ——, 2010: The position of the midlatitude storm track and eddy-driven westerlies in aquaplanet AGCMs. *J. Atmos. Sci.,* **67,** 3984–4000.

Medeiros, B., B. Stevens, I. M. Held, M. Zhao, D. L. Williamson, J. G. Olson, and C. S. Bretherton, 2008: Aquaplanets, climate sensitivity, and low clouds. *J. Climate,* **21,** 4974–4991.

Miller, R. L., G. A. Schmidt, and D. T. Shindell, 2006: Forced annular variations in the 20th century Intergovernmental Panel on Climate Change Fourth Assessment Report models. *J. Geophys. Res.,* **111,** D18101, doi:10.1029/2005JD006323.

Nakamura, N., 1996: Two-dimensional mixing, edge formation, and permeability diagnosed in an area coordinate. *J. Atmos. Sci.,* **53,** 1524–1537.

——, and A. Solomon, 2010: Finite-amplitude wave activity and mean flow adjustments in the atmospheric general circulation. Part I: Quasigeostrophic theory and analysis. *J. Atmos. Sci.,* **67,** 3967–3983.

——, and D. Zhu, 2010: Finite-amplitude wave activity and diffusive flux of potential vorticity in eddy–mean flow interaction. *J. Atmos. Sci.,* **67,** 2701–2716.

Neale, R., and B. J. Hoskins, 2000: A standard test for AGCMs including their physical parametrizations. II: Results for the Met Office model. *Atmos. Sci. Lett.,* **1,** 108–114.

Newman, M., and P. D. Sardeshmukh, 2008: Tropical and stratospheric influences on extratropical short-term climate variability. *J. Climate,* **21,** 4326–4347.

Previdi, M., and B. G. Liepert, 2007: Annular modes and Hadley cell expansion under global warming. *Geophys. Res. Lett.,* **34,** L22701, doi:10.1029/2007GL031243.

Ring, M. J., and R. A. Plumb, 2007: Forced annular mode patterns in a simple atmospheric general circulation model. *J. Atmos. Sci.,* **64,** 3611–3626.

——, and ——, 2008: The response of a simplified GCM to axisymmetric forcings: Applicability of the fluctuation–dissipation theorem. *J. Atmos. Sci.,* **65,** 3880–3898.

Rivière, G., 2011: A dynamical interpretation of the poleward shift of the jet streams in global warming scenarios. *J. Atmos. Sci.,* **68,** 1253–1272.

Robinson, W. A., 2000: A baroclinic mechanism for the eddy feedback on the zonal index. *J. Atmos. Sci.,* **57,** 415–422.

Seager, R., and Coauthors, 2007: Model projections of an imminent transition to a more arid climate in southwestern North America. *Science,* **316,** 1181–1184.

Sigmond, M., and Coauthors, 2004: A simulation of the separate climate effects of middle-atmospheric and tropospheric CO_2 doubling. *J. Climate,* **17,** 2352–2367.

Solomon, A., G. Chen, and J. Lu, 2012: Finite-amplitude Lagrangian-mean wave activity diagnostics applied to the baroclinic eddy life cycle. *J. Atmos. Sci.,* **69,** 3013–3027.

Vallis, G. K., E. P. Gerber, P. J. Kushner, and B. A. Cash, 2004: A mechanism and simple dynamical model of the North Atlantic Oscillation and annular modes. *J. Atmos. Sci.,* **61,** 264–280.

Wittman, M. A. H., L. M. Polvani, and A. J. Charlton, 2007: The effect of lower stratospheric shear on baroclinic instability. *J. Atmos. Sci.,* **64,** 479–496.

Wu, Y., R. Seager, M. Ting, N. Naik, and T. A. Shaw, 2011: Atmospheric circulation response to an instantaneous doubling of carbon dioxide. Part I: Model experiments and transient thermal response in the troposphere. *J. Climate,* **25,** 2862–2879.

Yin, J. H., 2005: A consistent poleward shift of the storm tracks in simulations of 21st century climate. *Geophys. Res. Lett.,* **32,** L18701, doi:10.1029/2005GL023684.